Eur Biophys J (2009) 38:1101–1114
DOI 10.1007/s00249-009-0515-0

ORIGINAL PAPER

Using a five-state model for fitting amplitude histograms from MaxiK channels: β-distributions reveal more than expected

Indra Schroeder · Ulf-Peter Hansen

Received: 23 April 2009 / Revised: 25 June 2009 / Accepted: 29 June 2009 / Published online: 21 July 2009

Abstract Fast gating of ion channels with rate constants higher than the corner frequency of the recording set-up can be evaluated by fitting so-called beta distributions to measured amplitude histograms. Up to now, this was preferentially done for O–C Markov sub-models with one open and one closed state. Here, a fit of the amplitude histograms from MaxiK (BK) single-channel records was achieved with a five-state model with two open and three closed states including three open–close transitions with rate constants higher than the corner frequency (20 kHz) of the inevitable low-pass filter of the recording system. The numerical values of the rate constants of these transitions enabled a nearly one-to-one relationship between typical regions of the histograms and the reactions in the Markov model. These characteristic features are the width of the peak at the apparent single-channel current, the side slopes at the open and at the closed peak, and the depth of the valley between the two peaks. However, the simplex routine alone was incapable of finding the solution but could do so if guided by hand along a suggested strategy.

Keywords Anti-aliasing filter · Fast gating · Open-channel noise · Selectivity filter · Single-channel current · Temporal resolution

I. Schroeder · U.-P. Hansen (✉)
Department of Structural Biology, University of Kiel, Leibnizstr. 11, 24098 Kiel, Germany
e-mail: uphansen@zbm.uni-kiel.de

Introduction

Ion channels in biological membranes fulfill various functions in a living cell, and thus they have always been in the focus of research. The unveiling of the crystal structure of KcsA (Doyle et al. 1998) has opened the way to an understanding of the biophysical mechanisms of ion transport at the molecular level. One of the most promising approaches is the application of molecular dynamics simulations (MD). They yield, e.g., detailed pictures of the interactions between the carbonyl groups in the selectivity filter and the permeant ion (Bernèche and Roux 2005; Miloshevsky and Jordan 2008) or of the role of salt bridges at the inner gate (Beckstein et al. 2003; Zimmerman 2004; Tayefeh et al. 2007) and of the helical screw movements of the S4 helix (Börjesson and Elinder 2008; Shafrir et al. 2008).

All these predictions of MD simulations have to be tested by physiological measurements. Ideally, these tests should be based not only on global properties, for example conductivity and selectivity, but also on something closer to the conformational changes in the channel protein. Much more stringent would be a comparison of gating behavior as predicted by MD simulations and as measured in a physiological experiment. Unfortunately, limited computing power restricts the description of temporal behavior by MD simulations to a very fast time scale. Nevertheless, there is hope that in the near future MD simulations which have now proceeded to some ten nanoseconds using conventional computer power (Tayefeh et al. 2007; Jeon and Voth 2008) may soon capture the temporal range above 1 μs when the full state-of-the-art computer power will be utilized. For smaller proteins with 30,000 atoms, for example Fip35, the range of 10 μs has already been reached (Freddolino et al. 2008) thus giving rise to the

hope that the temporal ranges of MD simulations and of physiological gating analysis will increasingly overlap.

In the light of the temporal constraints of MD simulations, the analysis of measured fast gating becomes more important. Until now, most investigations have dealt with gating in the range of milliseconds, partially because of limited temporal resolution but mainly because this kind of gating is of great medical (Lehmann-Horn and Jurkatt-Rott 1999; Ashcroft 2006) and biological (Blatt 2004; Hedrich and Marten 2006) interest. The value of the analysis of fast gating for the understanding of the biophysics of ion transport became apparent in studies of the stepwise opening of the selectivity filter in *Shaker* (Zheng and Sigworth 1997; Zheng et al. 2001) or of ion-depletion-induced fast gating in MaxiK (BK) channels (Schroeder and Hansen 2007, 2008). The model emerging from the analysis in MaxiK was in agreement with the results of MD simulations of Bernèche and Roux (2005) and Miloshevsky and Jordan (2008). These simulations predicted that the electrostatic repulsion of the (negatively charged) carbonyl groups in the selectivity filter causes an outward deflection of these groups when the compensating force of the permeating cations is weakened under ion depletion (Zhou et al. 2001; Yellen 2001).

There are four major approaches to the analysis of fast gating:

1 fitting beta distributions to measured amplitude histograms (FitzHugh 1983; Yellen 1984; Heinemann and Sigworth 1991; Klieber and Gradmann 1993; Tsushima et al. 1996; White and Ridout 1998);
2 the direct fit of the time series (HMM fit, Albertsen and Hansen 1994; Michalek et al. 2000; Fredkin and Rice 2001; Venkataramanan and Sigworth 2002);
3 fitting of 2D-dwell-time histograms (Magleby and Song 1992; Huth et al. 2006, 2008); or
4 power spectrum analysis (Sigworth 1985; Heinemann and Sigworth 1988).

The range around 1–10 μs^{-1} (where rotations in peptide chains seem to occur, Fierz et al. 2009) can be reached by means of beta distributions (Weise and Gradmann 2000; Schroeder and Hansen 2006, 2007, 2008), by fitting of 2D-dwell-time histograms (Magleby and Song 1992; Huth et al. 2006, 2008), or by power spectrum analysis (Heinemann and Sigworth 1988). In many cases, the model curves used to fit the experimental data are generated by means of simulations. This often is the most convenient way of overcoming the mathematical problems of including multi-state Markov models, filter response, sampling interval, and noise.

Here, we show that three fast gating processes with rate constants from 0.5 to 10 μs^{-1} can be revealed from an analysis of the amplitude histograms measured in MaxiK (BK). Until now, the analysis of amplitude histograms was usually based on a two-state sub-model for the description of the main peak at the apparent open-point histogram. This was sufficient for determination of the true single-channel current and the rate constants of the fastest gating process in MaxiK channels (Schroeder and Hansen 2006, 2007, 2008). Now, we have found that it is quite easy to fit beta distributions to complex full-amplitude histograms as they were obtained from MaxiK channels. The fit can be based on multi-state Markov models of gating if done along an appropriate strategy. This results from the very intriguing finding of a very close relationship between characteristic regions of the amplitude histograms and the rate constants of a Markov model.

Generally, evaluation of multi-state Markov models was considered to be a major strength of 2D-dwell-time histograms (Moss and Magleby 2001; Rothberg and Magleby 1999) or of the direct fit of the time series (HMM fit, Farokhi et al. 2000; Zheng et al. 2001). However, we found that the analysis of amplitude histograms requires much less computing time than, for instance, 2D-dwell-time analysis does (Huth et al. 2006, 2008). In the literature, two kinds of gating contributing to the shape of amplitude histograms can be found: fast gating not too far above the corner frequency of the filter leading to skewed amplitude histograms (Yellen 1984; Heinemann and Sigworth 1991) and very fast gating far above the filter frequency resulting in nearly Gaussian distributions. This type is less obvious as it broadens the inevitable amplitude distribution resulting from the baseline noise without major effect on the shape (Weise and Gradmann 2000; Schroeder and Hansen 2007, 2008). Sometimes a transition from the Gaussian type to the skewed type can be observed as found in *Chara* after addition of verapamil (White and Ridout 1998).

Under optimum experimental conditions (high single-channel currents in 400 mM KCl), we found that both types of gating coexist in MaxiK (or BK) channels and can be evaluated: one very short and one short closing interrupting the main open state and one short opening interrupting the main closed state. A five-state Markov model with two open and three closed states could fit these amplitude histograms. The fits yielded one pair of "very fast" rate constants (around 5 μs^{-1}) for the main peak at the apparent open level, and two pairs of "fast" rate constants (around 0.5 μs^{-1}) closer to the corner frequency of the low-pass filter (20 kHz). The latter were obtained from the side lobes of the peaks related to the apparent open and the closed level. One pair of slow rate constants (around 1 ms^{-1}) was used to adjust the height of the valley between the C and O peaks. Probably there are more slow reactions, which, however, cannot be resolved by the analysis of amplitude histograms, and would require a subsequent fit with other methods.

Materials and methods

Electrophysiology

Patch clamp measurements were performed on inside-out patches of HEK293 cells, stably expressing a h-MaxiK (BK) α-GFP construct and the β1-subunit (Lu et al. 2006). The bath and pipette solution contained 400 mM KCl plus 2.5 mM $CaCl_2$, 2.5 mM $MgCl_2$, and 10 mM HEPES. pH was titrated with KOH to 7.2. Patch electrodes were made from borosilicate glass (Hilgenberg, Malsfeld, Germany) coated internally with Sigmacote (Sigma, Deisenhofen, Germany), drawn on a L/M-3P-A puller (Heka, Lambrecht, Germany) and had a resistance of about 6 MΩ in 400 mM KCl. Drying of the pipettes at 55°C overnight after pulling increased seal probability and resistance up to 100 GΩ (Huth et al. 2008). Single-channel currents under steady-state conditions were recorded by a Dagan 3900A amplifier (Dagan, Minneapolis, Minnesota, USA) with a four-pole anti-aliasing filter (Bessel) of 20 kHz. Data were stored on disk with a sampling rate of 200 kHz and analysed with custom-made programs and Origin (see below).

Baseline drift, membrane flickering and other artifacts would distort the amplitude histograms and would lead to wrong results of the beta fit. Furthermore time series with sublevels have to be excluded from the analysis. However, this does not hold for incomplete short openings and closings related to fast gating as described in Fig. 1b, d, below. Thus, all data had to be closely inspected and cleaned manually from sections showing these kinds of artifact by means of the software Kiel-Patch. The legitimacy of this approach was considered for instance by Sigworth (1985).

Definitions

I_{true} is the true single-channel current, which could be measured with a set-up with sufficient bandwidth. I_{app} is the apparent single-channel current, which is obtained from an evaluation of the measured time series. Detailed definitions are given by Hansen et al. (1997, 2003) and Schroeder and Hansen (2006).

Baseline noise σ_B originates from the recording apparatus under the condition that a seal has been formed, but that there is no channel in the seal (or the channel is inactivated). It is not necessarily identical to the noise obtained from sections of a time series with channels in the non-conducting state. The latter may be broadened by fast flickering (Figs. 2, 3, below).

Very fast gating occurs at dwell times of at least 50 times shorter than the rise time of the filter of the amplifier (Fig. 2b, below). It is the origin of the reduction of I_{true} to I_{app}.

Fast gating leads to amplitude histograms with slopes deviating with a kink from the main peaks of the amplitude histograms. At least one rate constant of the related C–O transitions is above the fivefold value of the corner frequency of the filter. With filter, the inevitable low-pass filter (here four-pole Bessel filter) of the recording set-up is meant, not the selectivity filter of the channel.

Simulation of surrogate time series, generation and fitting of beta distributions

For the construction of the theoretical amplitude histograms, simulations instead of deterministic algorithms were used, because there is no straightforward procedure to calculate beta distributions for higher-order Bessel filters (Riessner 1998). Thus, time series and the corresponding amplitude histograms were simulated by the program Simulat (available at http://www.zbm.uni-kiel.de/aghansen/software.html) which employed the KISS generator (Marsaglia 2003) for creation of uniformly distributed random numbers.

The simulation algorithm has been described in previous papers (Blunck et al. 1998; Schroeder and Hansen 2006). It is similar to that suggested by Gillespie (1977) for chemical reactions. The generation and filtering (by a digital four-pole Bessel filter with a corner frequency f_C of 20 kHz) of the surrogate time series was done in continuous time. This allowed for dwell-times much shorter than the sampling interval (5 µs throughout this manuscript). Briefly, time series of single-channel current were simulated from a Markov model with a set of assumed rate constants k_{ij}. A pair of random numbers was generated for each transition in the Markov model: The first number selected the sink state of the next transition as weighted by the related rate constants. The second one determined the time w_k of the next jump from state i to state j from the inverted dwell-time histogram for the transitions from the source state. Knowing these times of the jumps (w_k), the value of the filtered time series at time the sampling point t was calculated by means of the equation:

$$I(t) = \sum_{\substack{k \\ w_k < t}} (I_{j,k} - I_{i,k}) + \sum_{\substack{k \\ t-45\Delta t_S < w_k < t}} (I_{j,k} - I_{i,k})(g(t - w_k) - 1) \quad (1)$$

where $I_{j,k}$ is the nominal current of state j at jump time w_k. The filter response $g(t)$, sampled every $\Delta t_S = 1/(28 f_C)$ µs (being 1.8 µs for a filter with a corner frequency of $f_C = 20$ kHz), was stored on the computer. Intermediate values were obtained by interpolation. The first sum in Eq. 1 could be calculated iteratively. The range of the second sum was kept finite by excluding all responses

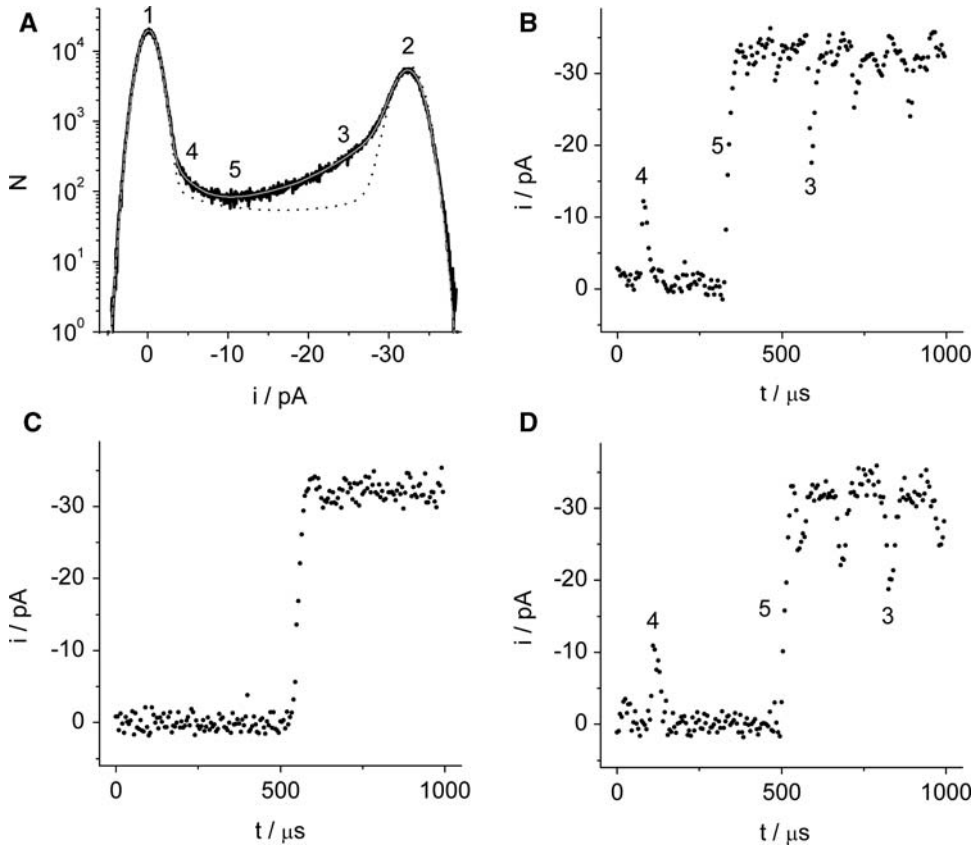

Fig. 1 **a** Amplitude histogram of MaxiK obtained in symmetric 400 mM K^+ at −120 mV with a 20-kHz four-pole Bessel filter and a sampling rate of 200 kHz fitted by the five-state model OCOZZ (Eq. 2). The *solid gray line* coinciding with the measured data (*black*) is the theoretical curve calculated from the data given in Table 1, column "Fig. 1". The *dotted black line* has been obtained by setting $k_{a3} = 0$ and $k_{1b} = 0$. σ_B was 1.00 pA, $I_{true} = 36.5$ pA, $I_{app} = 32$ pA. **b**, **d** Occurrence of incomplete transitions related to the side slopes (*regions 3 and 4*) in measured (**b**) and simulated (**d**) time series. **c** Simulations without the transitions from C1 to Ob and from Oa to C3 ($k_{1b} = 0$ and $k_{a3} = 0$, *dotted line* in (**a**)) led to elimination of the short peaks of the incomplete transitions. The rate constants for the simulation were obtained from the fit in **a**. The *dots* represent individual samples with a distance of 5 µs

whose contributions had decreased below one bit. At high rate constants, there were many jumps at times, w, located between the sampling points t resulting in very long times for generation of a single times series (up to several seconds).

From the surrogate time series obtained by the above algorithm, the amplitude histogram (beta distribution) was generated. The noise of the recording apparatus was introduced either by a convolution of this amplitude histogram and the Gaussian amplitude histogram of the baseline noise or by adding a pre-filtered noise time series directly to the simulated time series.

Because there is no simple analytical approach to calculation of beta distributions (Riessner 1998), the test of the reliability of the results, i.e., finding the allowed range of rate constants for a measured amplitude histogram, can be done only by an extremely time-consuming method as follows: Change the value of one rate constant obtained from the best fit by hand and keep it fixed during subsequent runs of fitting. These runs seek to compensate the error induced by the manual change of this rate constant by readjusting the other rate constants. The allowed range is given by the maximum deviations of the manually changed rate constant, which can still be compensated. Repeating this approach for all rate constants (for one data point) can take a week or more. Thus, the researcher has to make a decision of whether the scientific output is worth the efforts.

A strategy guide for fitting beta distributions is given in the Appendix.

Results and discussion

Characteristic features of MaxiK amplitude histograms

Figure 1a shows an amplitude histogram from a single MaxiK (or BK) channel measured with a four-pole Bessel filter of 20 kHz. It has been found that this histogram and nearly all other amplitude histograms obtained from

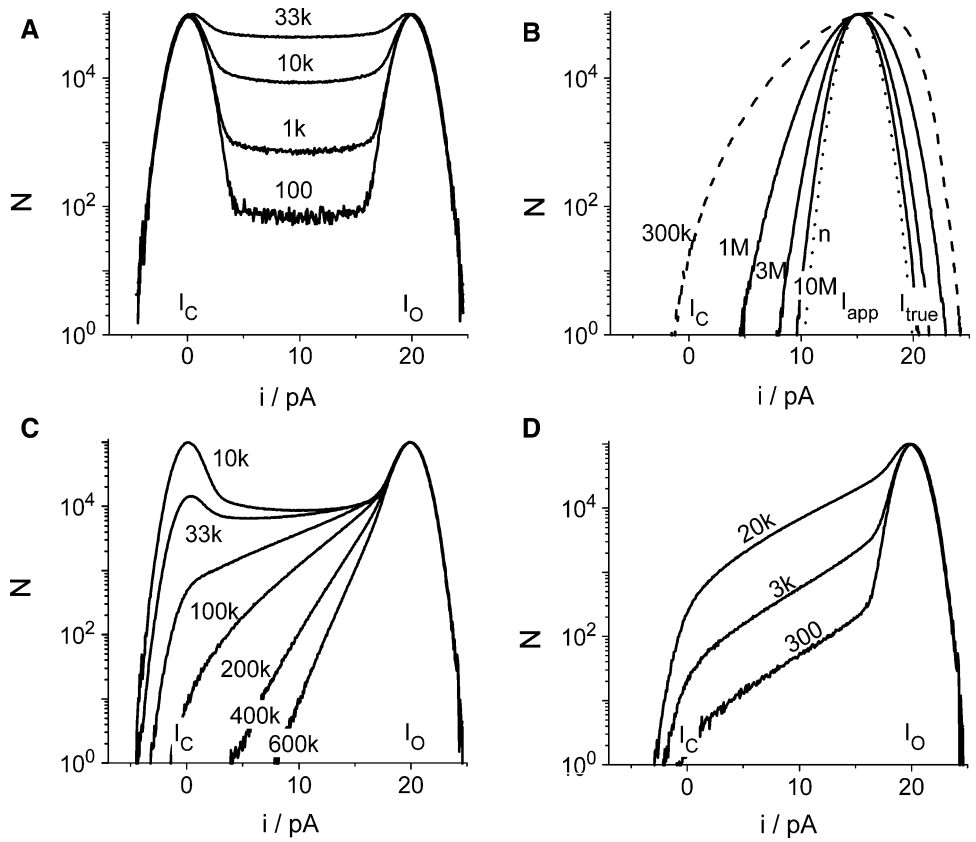

Fig. 2 Prototypes of beta distributions as generated from C–O models with different rate constants. The sampling frequency was 200 kHz, and the length of the simulated time series was 5×10^6 data points, filtered by a Bessel filter of 20 kHz. **a** Slow gating with $k_{CO} = k_{OC}$ ranging from 100 s^{-1} to 33,000 s^{-1} as indicated above the curves. **b** Very fast gating with $k_{CO} = 3k_{OC}$. k_{CO} is written next to the curves. The *dotted curve* labelled "*n*" presents the baseline noise. I_C, I_{app} and I_{true} indicate the current values for the closed state, the apparent open and the true open state, respectively. I_O is used, when the open level may be I_{app} or I_{true} depending on whether there is undetected additional very fast gating in a C–O–C model. **c** and **d** illustrate the determinants of the amplitude histograms generated by fast gating. **c** Influence of k_{CO} (written next to the curves) on the slope with $k_{OC} = 10{,}000$ s^{-1}. k_{CO} determines the slope without exerting an influence on the position of the "kink" where the slope deviates from the Gaussian main peak. **d** Influence of k_{OC} (written next to the curves) on the "kink" with $k_{CO} = 140{,}000$ s^{-1}. The slope is not influenced by the rate constant k_{OC}

MaxiK under similar conditions are composed of five characteristic regions. The observation of all five regions requires a good signal-to-noise ratio as found at high single-channel currents (e.g. with 400 mM KCl on either side of the membrane). The basic features (labelled in Fig. 1a) are:

1 the narrow peak at the closed level;
2 the broadened peak at the apparent open level;
3 the adjacent slope on the left-hand side of the O-peak;
4 the adjacent slope at the right-hand side of the C-peak; and
5 the height of the minimum between the peaks.

The amplitude histogram in Fig. 1a was fitted with a branched five-state model named OCOZZ by means of the procedure described in the Appendix. The state label "Z" indicates that the two closed states (C2, C3) are in parallel

$$Ob \underset{k_{1b}}{\overset{k_{b1}}{\rightleftharpoons}} C1 \underset{k_{a1}}{\overset{k_{1a}}{\rightleftharpoons}} Oa \begin{matrix} \overset{k_{a2}}{\rightleftharpoons} C2 \\ \underset{k_{3a}}{\overset{k_{a3}}{\rightleftharpoons}} C3 \end{matrix} \quad k_{2a} \tag{2}$$

The closed states C*i* ($i = 1$–3) are labelled by numbers, the open states O*j* ($j =$ a, b) by letters. The rate constants obtained from the fit of the histogram in Fig. 1 are given in Table 1 below. The scheme in Eq. 2 is in agreement with the finding of Moss and Magleby (2001) that there are no transitions between short *C* (<10 μs) and short *O* (<100 μs) states in the 2D-dependency plots from MaxiK. The temporal range suggests that these short-short transitions would correspond to C3–Ob transitions in Eq. 2. But they cannot occur in the model because C1 and Oa separate them.

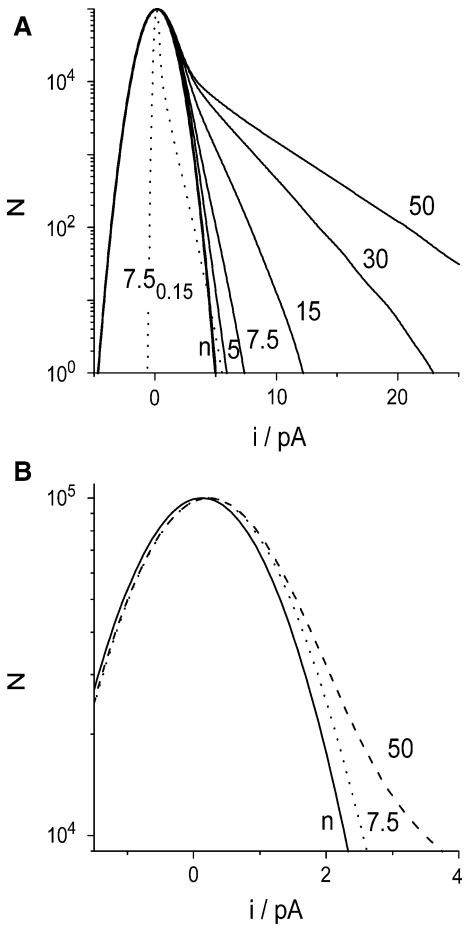

Fig. 3 **a** Partial amplitude histograms showing the influence of the signal-to-noise ratio i/σ on the observability of the side slope of the closed peak as studied by means of simulated data using a two-state model (Eq. 3) with $k_{CO} = 8{,}000\ s^{-1}$ and $k_{OC} = 400{,}000\ s^{-1}$. The numbers written next to the curves give the single-channel current i in pA. Here, this is equal to the ratio i/σ_B for the index-free numbers because σ_B is 1 pA. "*n*" labels the histogram caused by baseline noise with $\sigma_B = 1$ pA. The *dotted line* in (**a**) labelled $7.5_{0.15}$ was obtained with a current of 7.5 pA and $\sigma_B = 0.15$ pA resulting in the ratio $i/\sigma_B = 50$. **b** Enlarged presentation of the peak region in (**a**) for the three curves labelled *n*, $i/\sigma_B = 7.5$ and $i/\sigma_B = 50$. Sampling rate was 200 kHz. The four-pole Bessel filter was set to 20 kHz cut-off frequency

The individual components of MaxiK amplitude histograms

In most cases observed in MaxiK channels, the individual transitions of the five-state model of Eq. 2 can be well distinguished in the measured amplitude histograms. Each of the characteristic elements of the amplitude histogram in Fig. 1a can be generated by a simple two-state C–O model

$$O \underset{k_{CO}}{\overset{k_{OC}}{\rightleftharpoons}} C \tag{3}$$

The different types of histograms are shown in Fig. 2.

Slow gating

The histograms generated by slow gating are well known. The two peaks in Fig. 2a are located at the nominal currents of the closed and open state, and their curve shapes are determined by the Gaussian distribution of the baseline noise. In the related time series (not shown), we see clear assignments to the O and C levels. The relative heights of the two peaks are determined by the ratio k_{OC}/k_{CO}. Important also is the height $f(i)$ of the valley between the peaks (region 5 in Fig. 1a). It is determined by the number of transitions of upward ($[C]k_{CO}$) and of downward ($[O]k_{OC}$) jumps and by the difference in the times s when the filter response reaches the current values i and $i + \Delta i$, respectively.

$$f(i) = \frac{[C]k_{CO}(s_u(i) - s_u(i+\Delta i)) + [O]k_{OC}(s_d(i+\Delta i)) - s_d(i))}{\Delta T} t_M \tag{4}$$

where $s_u(i)$ is the time when the Bessel filter response reaches the current i in an upward jump and s_d when the current i is reached in a downward jump. These times have to be calculated from the inverted response function of the filter. Δi is the bin width of the amplitude histogram. ΔT is the sampling interval (5 μs) and t_M the length of the record.

In an infinitesimally fast recording system, the height of the valley between the peaks would be zero, because the output signal immediately jumps from O to C with $s(i) = s(i + \Delta i)$. In a real system, these jumps have to occur along the filter response (data points on the complete transitions between the O and C levels in Fig. 2), thus filling the gap between the O and C peaks. This occurs also in the case of very slow gating, but less often. Thus, the height of the minimum is a means of determining the absolute values of k_{CO} and k_{OC} for a given low-pass filter (Eq. 4).

Very fast gating

Gating with rate constants more than about 50 times the corner frequency of the filter is called "very fast gating". It merges the amplitudes histograms of the open and closed state (which are well separated in Fig. 2a) into one peak: The shape is more or less Gaussian resulting from the fact that gating is much faster than the filter frequency (Feller 1968) for k_{CO} greater than 1–3 μs^{-1} (50–150 times the corner frequency of the filter). Lower values of k_{CO} (0.3 μs^{-1}, dotted curve) show characteristics of the shape of only "fast" gating in Fig. 2c (i.e., they are visibly skewed), but the kink visible in Fig. 2c, d is not pronounced because of the small difference between k_{OC} and k_{CO}. The peak of the distributions in Fig. 2b is located at the "apparent" single channel-current I_{app} which is smaller

Table 1 Rate constants obtained from fitting the amplitude histograms in Figs. 1 and 4 measured in MaxiK in symmetrical 400 mM KCl

	Fig. 1	Fig. 4A			Fig. 4B	
		a	b	c	a	b
V/mV	−120	−20	−20	−20	−80	−80
Fit quality	Ok	Ok	Ok	Ok	Ok	Failed
Baseline/pA	0	0	−0.063	−0.377	0	−0.377
σ_B/pA	1.00	1.08	1.08	1.03	1.13	1.00
I_{true}/pA	36.5	5.95	6.10	8.34	25.2	28.1
k_{b1}/s^{-1}	467,000		320,000	320,000	480,000	320,000
k_{1b}/s^{-1}	600		6,000	28,000	880	3,600 or 7,000
k_{1a}/s^{-1}	615	7,280	5,480	2,700	4,640	3,600
k_{a1}/s^{-1}	1,550	980	760	520	1,640	1,388
k_{a2}/s^{-1}	667,000		69,600	82,000	192,000	404,000
k_{2a}/s^{-1}	5,200,000		5,840,000	2,400,000	3,096,000	3,604,000
k_{a3}/s^{-1}	7,600	7,360	8400	4,000	3,680	4,000
k_{3a}/s^{-1}	181,000	209,200	216,400	180,000	132,000	128,000

The labels "a", "b", and "c" refer to the different parameter sets used to fit the same curve in Fig. 4A or Fig. 4B

Table 2 Rate constants of the model in Eq. 2 and single-channel current as obtained from the individual steps of the recommended fitting strategy for the related graphs in Fig. 5

Step	k_{2a}/s^{-1}	k_{a2}/s^{-1}	k_{3a}/s^{-1}	k_{a3}/s^{-1}	k_{a1}/s^{-1}	k_{1a}/s^{-1}	k_{1b}/s^{-1}	k_{b1}/s^{-1}	I/pA
A smooth					1,800	800			32
A dashed					180	80			32
B	4×10^6	553,000			291	105			36.5
C	5.2×10^6	667,000	140,000	8,200	220	90			36.5
D	5.2×10^6	667,000	140,000	8,200	219	85.5	700	200,000	36.5
E	5.2×10^6	667,000	140,000	8,200	526	205	700	200,000	36.5
F	5.2×10^6	667,000	181,000	7,600	1,550	615	600	467,000	36.5

than the true single-channel current I_{true} as given by the relationship:

$$I_{app} = \frac{k_{CO}}{k_{OC} + k_{CO}} I_{true} \tag{5}$$

Very fast gating cannot be observed directly in the measured time series because of the smoothing effect of the filter. Instead, a "noisy" signal occurs around the apparent single-channel current I_{app}. This signal increases the width of the apparent open-channel peak (Region 2 in Fig. 1a) as becomes obvious from a comparison of the peaks in Fig. 2a and Fig. 2b (i.e., it is one of the sources of open-channel noise; Sigworth 1985; Heinemann and Sigworth 1991). The influence of fast gating on the shape of the apparent open-channel peak can be used to determine the rate constants k_{CO} and k_{OC} (Schroeder and Hansen 2006, 2007, 2008) and the true single-channel current I_{true} (Eq. 5).

It may be regarded as surprising that fitting of curves like those in Fig. 2b can lead to the evaluation of rate constants up to 500 times faster than the corner frequency of the filter. This is based on the feature that the "10 M" curve in Fig. 2b is clearly broader than the "n" curve. The n curve (baseline noise, σ_B) can be obtained from the noise of a channel-free section of the patch clamp time series (but not always from the C level, see Figs. 3, 4). Fig. 2b also shows that the dependence of the width on the amplitude histogram on the rate constants becomes quite flat around 10 μs^{-1} as shown by Schroeder and Hansen (2009). Thus, the scatter of the determination of rate constants rapidly increases in that region of very fast gating.

Furthermore, at values of k_{OC} around 10 μs^{-1}, the Schottky noise (Sigworth 1985) resulting from the low number of ions per open-event (a single-channel current of 16 pA implies that ten ions are transferred during an open event of 0.1 μs) might also have an effect on the shape of the open-level peak. However in most cases, this can be ignored as discussed by Schroeder and Hansen (2009).

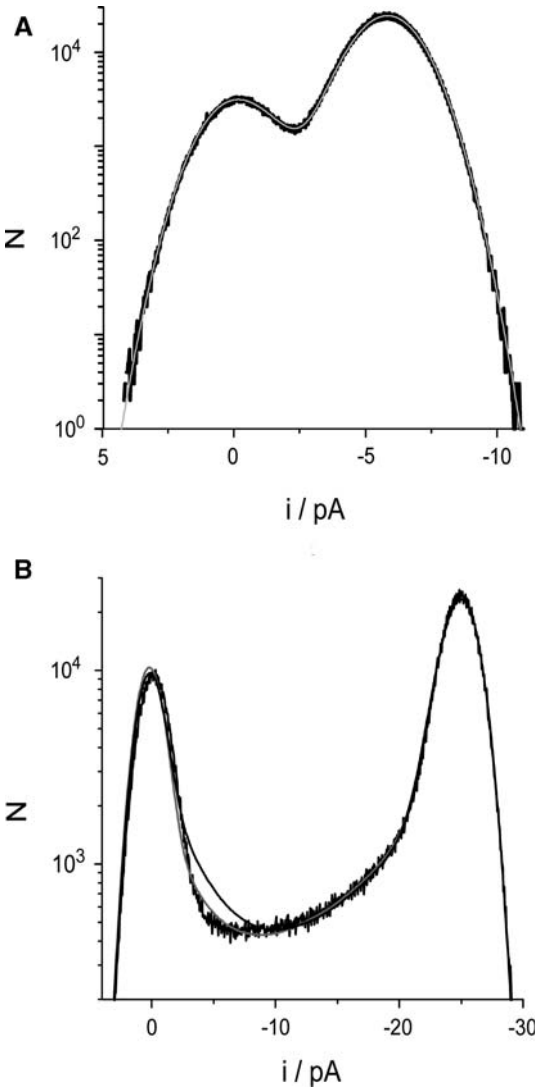

Fig. 4 Limitations of the analysis demonstrated for amplitude histograms measured in MaxiK measured at −20 mV in 400 mM K^+. **A** Superposition of measured data (*black*) and three fits (*gray*, the three theoretical curves coincide and are not distinguishable) with different assumptions about the relative contributions of C1–Ob gating and baseline noise σ_B to the baseline and to the apparent σ of the C-peak. In Table 1 the parameters of these three different fits are given in columns "Fig. 4A, a–c". **B** In contrast, if the i/σ_B ratio ($I_{true} = 25.2$ pA, $\sigma = 1.13$ pA) is high enough (at −80 mV, measured data in *scattery black*) there is a unique good fitting result (curve not shown for the sake of clarity; the parameter set of the fit is given in Table 1, column "Fig. 4B, a"). All attempts to merge baseline noise and C1–Ob gating fail, e.g. when σ_B is reduced from 1.13 to 1.00 pA (the related parameter sets of the fits are given in Table 1, column "Fig. 4B, b"). The smooth curves were obtained with the values in Table 1, column "Fig. 4B, b" with $k_{1b} = 3{,}600\ s^{-1}$ (*gray*) or $7{,}000\ s^{-1}$ (*black*)

Fast gating

The new features in Fig. 1a are the side slopes (regions "3" and "4"). Figures 2c, d show how the side slopes are related to the rate constants k_{a3}, k_{3a} of the Oa–C3 transitions in the model of Eq. 2. The rate constant k_{a3} goes up to 30 times the filter corner frequency. At the closed-level side the rate constants k_{1b} and k_{b1} generate the side slopes. The side slopes arise from jumps from source state R to sink state S, which are too short for the output of the recording apparatus to reach the level of the sink state. It stops on this way depending on the ratio of f_c/k_{sr} (with f_c being the corner of the filter) and returns to the level of the source state. This can be observed in time series of measured data (Fig. 1b) and of related simulated data (Fig. 1d), which have been generated from the rate constants of the fit (gray) in Fig. 1a. If the related rate constants are omitted in the simulations ($k_{a3} = k_{1b} = 0$, dotted line Fig. 1a), these incomplete openings and closings are not observed (Fig. 1c).

These short and relatively infrequent closings/openings, we call "fast gating" in contrast with "very fast gating" as found at the apparent open-level peak (Region 1 in Fig. 1a, Fig. 2b). Fast gating is related to the incomplete transitions shown in Figs. 1b, d. Here, the duration in the source state is still long enough (k_{OC} is slow, $10{,}000\ s^{-1}$) that the related gating does not lead to a strong shift in the current levels (but see Fig. 3b and Table 1 "Fig. 4B, b"). In models with quite fast source-sink transitions (e.g. Oa–C2 transitions), the source-level can also be an apparent level (i.e. the apparent O level I_{app} in Fig. 2b). The dotted line in Fig. 1a also does not match the peak of the O level. This misfit results from refugees, namely the data points now expelled from the areas related to the side slopes.

There is one feature in Fig. 1b and d which supports the view that the incomplete transitions are not jumps to putative sublevels of conductance: The number of data points on the leading edge is less than on the trailing edge in both the measured and simulated data. This results from the fact that the filter starting from the source state gets an input signal, which initiates a jump to the next full level, but on its way it is stopped when the dwell-time of the sink state ends (k_{b1} or k_{3a}). On the way back to the source state, the slope is determined by the smaller difference between the point of return and the level of the source state. Thus, more data points are found on the flatter trailing edge.

Fortunately, there is a quite simple relationship between the rate constants and the characteristic features of these side slopes. The gradient of the slope is determined by k_{SR} and is independent of k_{RS} (Fig. 2c) with R labelling source and S sink. The kink where the slope deviates from the noise-born and/or very-fast-gating-born main peak is determined by k_{RS} and is independent of k_{SR} (Fig. 2d).

Caveats at low signal-to-noise ratios

At low membrane potentials, the distance between the O level and the C level becomes narrow. This leads to

problems when the rate constants of the transitions between C1 and Ob (Eq. 2) are to be evaluated. The problem is illustrated by simulated data in Fig. 3 and by measured data in Fig. 4.

Figure 3 shows simulated amplitude histograms of the closed peak and the adjacent side slope obtained from a truncated model (Eq. 3) with fixed rate constants $k_{CO} = 8{,}000\ s^{-1}$ and $k_{OC} = 400{,}000\ s^{-1}$, typical values for MaxiK (or BK) channels found at different nominal single-channel currents. This roughly corresponds to Region 4 in Fig. 1a and (with reversed roles for O and C) to the "400 k" curve in Fig. 2c. At small currents, there is not such a characteristic kink as is observed at high currents (higher than 7.5 pA in Fig. 3a). At lower currents, the peak of the baseline noise and the effect of the fast gating are merged in a broadened distribution. Although this distribution is slightly skewed, it can hardly be distinguished from a Gaussian distribution of the baseline noise, especially when only the top of the peak can be distinguished from the horizontal part of the five-state model (Figs. 1a, 2a). Figure 3b gives a clearer picture of the effect of fast gating. In the presence of fast gating (curves with 7.5 and 50 pA) the peak of the C level distribution is slightly shifted towards higher currents. The histogram related to 7.5 pA is broadened and almost looks like a Gaussian distribution. This merges the effect of fast gating into apparent baseline noise.

The dotted line in Fig. 3a labelled "$7.5_{0.15}$" demonstrates that the signal-to-noise ratio i/σ_B is the sole determinant of observability. The pair $i = 7.5$ pA, $\sigma_B = 0.15$ pA has the same i/σ_B ratio as the pair $\sigma_B = 1$ pA, $i = 50$ pA in (A), thus resulting in the same shape of the histograms (after spreading the abscissa for the dotted curve by a factor of 1/0.15).

The above findings in the simulated data pose the following problem for the experimenter: The width σ_B of the baseline noise is normally determined from the width of the measured C level distribution. According to Fig. 4a, this level may already include the effect of fast gating. If under these conditions (i.e., the C-peak is used for the determination of σ_B) the fit would lead to the probably false conclusion that fast gating at the C-side is not present. A way out is to determine σ_B from reliably channel-free sections of the time series. They may be obtained by blocking the channel by TEA, Ba^{2+} or other agents. Another approach may compare the σ_B obtained at different membrane potentials/single-channel currents. In either case, it has to be tested on channel-free preparations that these agents or membrane potential do not influence σ_B.

The evaluation of amplitude histograms measured in MaxiK (or BK) channels at −20 mV suffers from this problem. The signal-to-noise ratio of the time series corresponds to the 7.5 pA curve in Fig. 3a, b. In Fig. 4a, three fits of such an amplitude histogram are shown. The existence of three fits is not visible in Fig. 4a because they all lead to virtually identical theoretical curves which are presented by the gray curve. However, the fit parameters are quite different (Table 1, columns "Fig. 4A, a–c"). The fit parameters in column "Fig. 4A, a" in Table 1 have been obtained under the assumption that the baseline and σ_B can be determined from the C-peak. Under this assumption, fitting can be done in a three-state model with $k_{1b} = k_{a2} = 0$ suggesting that the C1–Ob and C2–Oa transitions do not occur. However, the column "Fig. 4A, b" shows that a slight shift in the putative baseline results in a fit which tolerates a value of k_{1b} which is slightly higher than the value of k_{1a}. Even worse, a good fit (all fits coincide with the gray curve in Fig. 4A) is obtained also with a tremendously higher k_{1b} implicating (unlikely) frequent transitions between C1 and Ob (column "Fig. 4A, c" in Table 1).

This uncertainty of the true level and noise of the baseline can become a serious problem. For instance, the equality of k_{1b} and k_{1a} is a salient feature of the discussion of the adequate Markov model, which will be presented in a subsequent paper. The comparison of the three sets of rate constants related to the histogram in Fig. 4A stresses the necessity of having channel-free records of the same patch, because all three solutions in Table 1 are indistinguishable when baseline level and noise can be estimated only from a C-peak like that in Fig. 4A.

This problem does not occur if the ratio i/σ_B is high enough as illustrated in Fig. 4B for an amplitude histogram obtained at −80 mV. For the histogram shown in Fig. 4B, a good fit of the histogram is obtained if $\sigma_B = 1.13$ pA and the baseline at 0 pA are estimated from fitting the Gaussian top of the C-peak. The rate constants are given in Table 1, column "Fig. 4B, a". In order to test whether a higher value of k_{1b} could be obtained by reducing σ_B (as in Fig. 4A, Table 1, column "Fig. 4A, a–c") σ_B was reduced from 1.13 to 1.00 pA, and the baseline was moved to −0.377 pA (in order to fit also the data points with small values of N on the left-hand edge). Figure 4B presents the good news that these fits are bad. This clear message results from the good i/σ_B ratio. The important characteristic is the kink where the slope related to C1–Ob gating separates from the Gaussian noise distribution (Fig. 3a, b at high currents, Fig. 2c, d and Fig. 4b). When this kink is no longer hidden by the histogram of the baseline noise (compare Fig. 3a), C1–Ob gating can be clearly identified by the fitting procedure, because in that case C1–Ob gating does not contribute to the width of the peak at the C level. Thus, at high i/σ_B ratios, the noise can be determined from the peak of the C level without interference from C1–Ob gating.

Model equivalence

The analysis described above is done on the basis of the OCOZZ model as given by Eq. 2, because this model yields a good decoupling of the individual components as shown in Fig. 2. This feature of the OCOZZ model is the basis for a quite straightforward fitting procedure as described in the Appendix. On the other hand, the researcher is not interested in a "convenient" model, but in a "true" model. "True" means that the states of the model and the transitions between them can be related to certain moieties and their dynamics in the channel protein.

Many Markov models are kinetically equivalent, i.e., they cannot be distinguished by means of a kinetic analysis of the measured time series. If models are equivalent, a transformation matrix S exists, which can transform the matrix K of rate constants k_{ij} of model A to the matrix Q of rate constants q_{ij} of model B (for details, see Kienker 1989)

$$S^{-1}KS = Q \tag{6}$$

The problem is to find S, which leads to extremely complex non-linear equations if the models have more than three states. Fortunately, the values of the rate constants at least in MaxiK are of such a kind that an approximate transformation of models is eased. For instance, the rate constants of the transitions Oa–C3 and Oa–C2 are fast or very fast, those of Oa–C1 are slow (see Eq. 2 and Table 1). This implies that modifications on the C1 side of Oa have little effect on the rate constants on the C2/C3 side. This enables splitting of the model in two sub-models which are transformed separately. One interesting transformation is the conversion of the model in Eq. 2 to the model COOZZ.

$$C1 \underset{q_{b1}}{\overset{q_{1b}}{\rightleftharpoons}} Ob \underset{q_{ba}}{\overset{q_{ab}}{\rightleftharpoons}} Oa \begin{array}{l} \overset{q_{a2}}{\rightleftharpoons} C2 \\ \overset{q_{2a}}{\rightleftharpoons} \\ \overset{q_{a3}}{\rightleftharpoons} \\ \underset{q_{3a}}{\rightleftharpoons} C3 \end{array} \tag{7}$$

The model of Eq. 2 implies that the inner gate of the channel has two independent open conformations which both open the way for the current. The conformation related to Ob is quite unstable, leading to incomplete openings (short pulses in Fig. 2b, d). The conformation related to Oa is related to the main open event of the inner gate. Its apparent lifetime is given by the inverse of k_{a1} (in the ms range). The interruption by fast gating as caused by the transitions to C2 are caused by flickering of the selectivity filter and must not be understood as closure of the inner gate in state Oa (Schroeder and Hansen 2007, 2008). The same is probably true for the fast Oa–C3 gating, but that still has to be verified.

The alternative model of Eq. 7 implies that Ob and Oa correspond to subsequently occurring configurations of the opening inner gate. When the inner gate opens, Ob is the first open configuration. It is still unstable and may close spontaneously via q_{b1}. The other possibility as provided by q_{ba} is the rearrangement to the more stable configuration Oa.

In a subsequent paper dealing with the voltage dependence of the rate constants, the equations for transforming the model of Eq. 2 into that of Eq. 7 will be given (i.e., the matrix S of Eq. 6 is presented) and the probability and the implications of these two models will be discussed.

Conclusions

Even though amplitude histograms have been used by different authors to determine gating parameters by means of various approaches (Yellen 1984; Heinemann and Sigworth 1991; Klieber and Gradmann 1993; Tsushima et al. 1996; White and Ridout 1998; Weise and Gradmann 2000; Schroeder and Hansen 2006, 2007, 2008), to our knowledge never more than one fast gating process has been revealed from the same histogram, even though both kinds of shapes have been reported. Sometimes the almost-Gaussian shape as caused by processes far above the filter frequency and the skewed (or "kinked") one as related to slower rate constants have been found in the same object, but separately under different conditions (Yellen 1984; White and Ridout 1998).

Here, we found that after increasing the signal-to-noise ratio by using high concentrations of the permeant ion (400 mM KCl) meticulous analysis of beta distributions proved to be more powerful than expected because it enabled evaluation of three fast gating processes with rate constants above the corner frequency of the filter and one slow gating process. The analysis of the very fast gating process leading to the open-point histograms with almost Gaussian shapes is of special importance because it enables estimation of the true single-channel current I_{true}. Often this kind of gating is the origin of negative slopes in the measured IV curves (Draber and Hansen 1994; Schroeder and Hansen 2007, 2008; Abenavoli et al. 2009).

The two processes called "fast gating" (Oa–C2 and C1–Ob in Eq. 2) lead to characteristics in the amplitude histograms, which are to some extent equivalent to one-dimensional dwell-time distributions (Colquhoun et al. 1996; Blunck et al. 1998). Dwell-time analysis is based on a plot where the number of events with a given dwell-time is plotted versus this dwell-time. The sub-histograms related to fast gating (Fig. 2c, d) give the number of events related to the short openings or closures shown in Fig. 1b, d. These pulses rise with the time constant of the anti-aliasing filter

until the ascent is stopped by the end of the dwell-time in Ob or in C3, respectively. Consequently, the height of these pulses (and thus the location on the abscissa of the amplitude histogram) is determined by the dwell-time in the short-lived states (as also calculated by Heinemann and Sigworth 1991). The difference from dwell-time analysis is that the sub-histograms correspond to dwell-time histograms, which are defined by the number of events, which have at least the dwell-time τ and not exactly the dwell-time τ (in the bins between τ and $\tau + \Delta\tau$, of course). The resulting shape of these incomplete openings and closings is a means of distinguishing them from sublevels, which have to be excluded from the analysed time series.

The benefit of the analysis by beta distributions is that it deals with those fast processes which can be determined by classical dwell-time analysis only with sophisticated (and more or less inefficient, Farokhi et al. 2000) correction algorithms (Milne et al. 1989; Crouzy and Sigworth 1990; Ball et al. 1993; Draber and Schultze 1994; Qin et al. 2000).

On the other hand, the analysis has been time-consuming. The stand-alone application of the Simplex algorithm (Caceci and Cacheris 1984) was restricted to the fit of the very fast gating processes related to the open-peak, and quite reliably delivered the rate constants k_{2a} and k_{a2}. It was nearly useless for the other rate constants. Thus, fitting had to be done by the procedure described in the Appendix. On a good day, four histograms could be fitted. On bad days, i.e., on days when histograms with bad signal-to-noise ratios like those in Fig. 4A had to be fitted, working on one histogram could take three days. This large effort resulted from the effect that a unique solution was not found, and time was spent to find ranges of rate constants which were allowed (Fig. 4a) and which were not (Fig. 4b) in order to get a picture of how reliable the evaluated parameters were.

Despite this, in a subsequent paper analysis of the voltage dependence of the rate constants in MaxiK for the models in Eqs. 2 and 7 will be presented. We still feel that the method presented here can provide important insights when results dealing with protein dynamics (which may be obtained from MD simulations and fluorescence studies) have to be compared with the physiological behaviour of the channel. This is especially true as the fast and very fast gating effects determined from the analysis described here will be the first ones which may be predicted by MD simulations.

Acknowledgments This work was supported by the Deutsche Forschungsgemeinschaft Ha712/14-3. We are grateful to Axel Scheidig for continuous support, to Professor U. Seydel and Dr A. Schromm, Research Center, Borstel, for providing the cells, and to Sonja Vollbehr for taking care of the HEK cells.

Appendix: strategies for fitting beta distributions to measured amplitude histograms

The straightforward approach to evaluation of measured beta distributions would be automatic fitting of the amplitude histogram on the basis of an adequate Markov model. Unfortunately, the Simplex search routine (Caceci and Cacheris 1984) did not find the correct parameter set of five-state Markov models. It was only successful in the case of fitting distributions-per-level (open-point histograms, Schroeder et al. 2004, Schroeder and Hansen 2006, 2007, 2008, 2009) using 2 or 3-state models.

Because of this, fitting had to be done interactively between the computer and the human operator. A dialogue in the fitting program (bownhill.exe at http://www.zbm.uni-kiel.de/aghansen/software.html) allowed the optional entry of fixed variables (single-channel current, baseline, baseline noise and rate constants), the introduction of weighing factors, and, finally, the selection of "free" rate constants, which were subject to the optimization by the simplex algorithm. By virtue of the weak interference between the regions labeled in Fig. 1a, this strategy enabled the adjustment of certain regions in the amplitude histogram without seriously affecting those which had already been fitted correctly or which were not of actual interest.

Below, this strategy based on the model in Eq. 2 is illustrated for the amplitude histogram shown in Fig. 1a. The boxes in Fig. 5f denote the actual "region of interest" for each fitting step. They can also be interpreted as an approximate visualization of weighing factors used during for optional fitting by the computer.

Step A of the fitting routine starts with the slow C1–Oa transition of the model in Eq. 2 by adjusting k_{1a} and k_{a1} in the rate constant matrix. The other rate constants may be estimates obtained from previous fits or may be set to zero.

The best possible fit result with the other k's set to zero (thus essentially creating a two-state model) is shown as the solid curve in Fig. 5a: Only the closed peak (in the box) is fitted reasonably well. The misfit of the height of the open peak is necessary because, in the next step, the data points above the open peak are redistributed to broaden the open peak. The dotted line illustrates a subsequent enhancement of the misfit of the intermediate region between the O and C peak by manually reducing k_{1a} and k_{a1} by the same factor. This preserves the relative occupations of the C and O peak (Fig. 2a), but reserves space for adjustment of the side slopes (Fig. 2c, d) done in the next steps.

Step B (Fig. 5b) has to deal with the O peak because it comprises a large number of data points. Because the fitting routine consists of subsequent adjustment of specific parts of the full amplitude histogram, data points can be

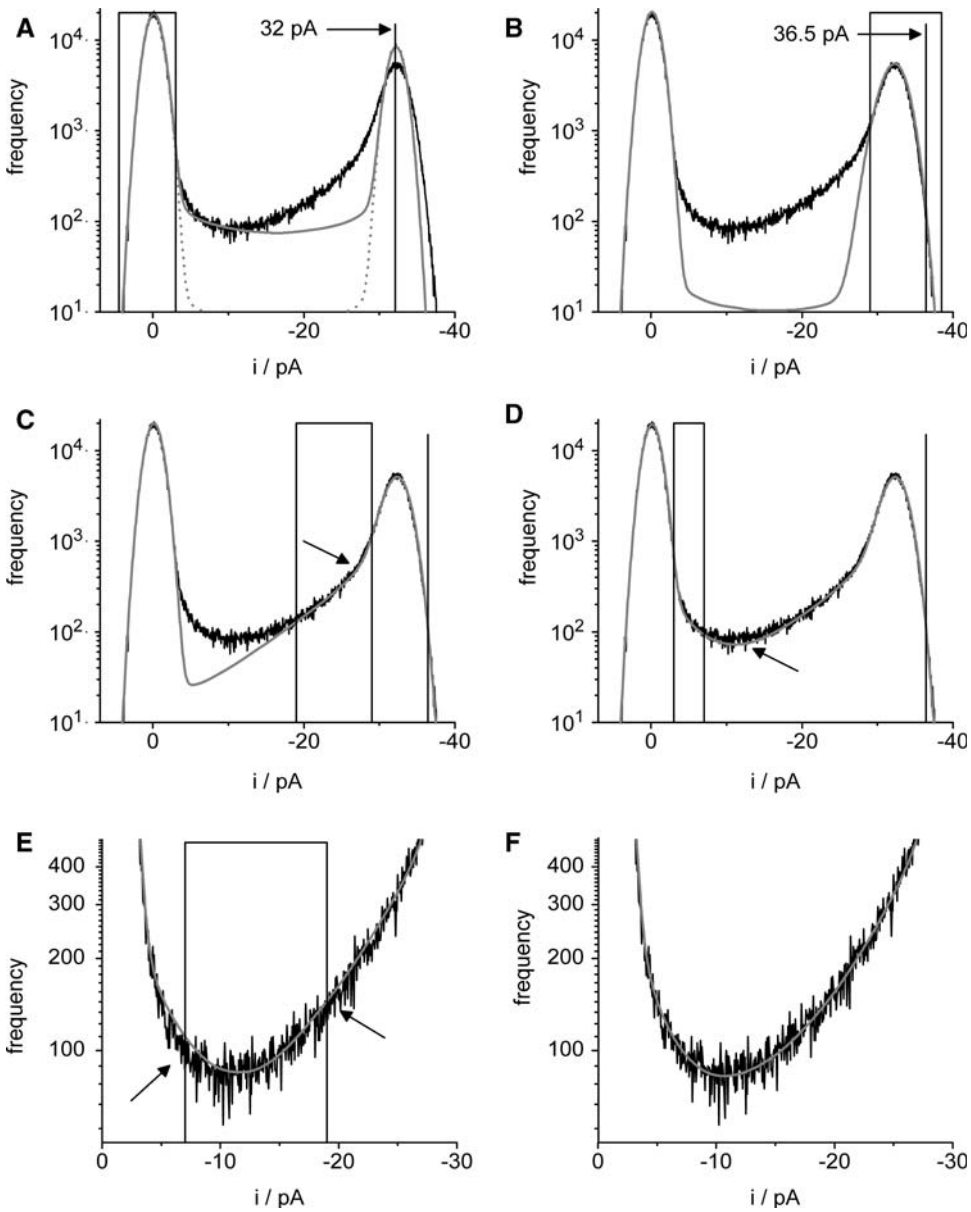

Fig. 5 Sequence of steps of the recommended fitting strategy as illustrated for the data in Fig. 1a measured from a single MaxiK channel in symmetrical 400 mM KCl at −120 mV membrane potential. Details are described in the text. The values obtained in the individual steps are given in Table 2

shuffled from regions just being fitted to those fitted before. This has a less destructive effect if data points are shuffled to the main peak from the smaller side slopes or from the valley.

The width of the O peak is determined by very fast gating (Fig. 2b). The values of I_{true}, k_{a2} and k_{2a} are adjusted until the region in Fig. 5b marked by the box is fitted satisfactorily. Here, the simplex algorithm works fine for k_{a2} and k_{2a} if I_{true} is fixed. The fit has to be repeated for different guesses of I_{true}. This can be guided by the error sum as described by Schroeder et al. (2006, 2007) or by a visual inspection of the fit result (which is more labour-intensive, but also more accurate). When the simplex algorithm is employed, weighting factors can be used to concentrate the calculation of the error sum to this region.

Step C deals with the soft slope near the open peak (box in Fig. 5c), again following the rule that those regions comprising more data points have to be fitted first. The adjustment of the steepness (Fig. 2c) of the slope via k_{3a} and of the location of the kink (arrow in Fig. 2C) via k_{a3} works best if done manually, because a parallel shift of the slope (adjusting k_{3a}) can be handled better by the superb image analysis software of the human brain than by crude error-sum calculations of the computer.

If the kink is close to the peak of the O distribution, fitting of the slope can also affect the shape of the main peak. Thus, k_{a2} and k_{2a} might have to be slightly readjusted. This can be done by the simplex algorithm. Because data points are shifted between O and C, a slight adjustment of k_{a1} and k_{1a} may also become necessary.

Step D (Fig. 5D) employs the same strategy as step C, but now applied to the fitting of the side slope of the C level by means of k_{1b} (gradient) and k_{b1} (location of the kink). Again, a slight adjustment of k_{a1} and k_{1a} may also become necessary to correct the fit at the C and O peaks. At the end of step D, the intermediate region (indicated by an arrow in Fig. 5d) still shows a misfit.

Step E achieves the closure of this gap by increasing k_{a1} and k_{1a} while maintaining their ratio.

Step F deals with the final corrections. Step E creates new error zones because lifting the valley (Fig. 5d, arrow) also moves up the side slopes (Fig. 5e, arrows). This has to be compensated by increasing k_{3a} (and/or k_{b1}), which may again sink the valley. This coupling between slope and valley may sometimes lead to repetitive readjustments of the rate constants of the slopes and of the valley. Nevertheless finally, a perfect fit can be obtained as shown in Fig. 5f.

The need for iterative repetitions of the above procedure depends on how strongly the individual components of the amplitude histogram are separated. In the best case (at high single-channel currents), the routine can be finished after the first run. In worse cases, several readjustments using the above scheme may become necessary. At the end of the manual fitting routine, an automatic run with the simplex algorithm may result in fine adjustment (or in a stray run).

It may be desirable to have an algorithm which automatically does the fit along the list of steps given above. The salient feature for such a fully automatic fitting routine would be a new error criterion, which would accept a parallel line as a preliminary result. After having achieved the parallel location of the hypothetical and measured side slopes (regions 4 and 3 in Fig. 1a) the theoretical slope should be shifted towards the measured one by adjusting k_{a3} (or k_{b1}). Programming of such an algorithm may become worthwhile if urgent scientific questions have to be answered by an intense application of the five-state analysis of beta distributions.

References

Abenavoli A, DiFrancesco M, Schroeder I, Epimashko S, Gazzarrini S, Hansen, UP, Thiel G, Moroni A (2009) Fast and slow gating are inherent properties of the K^+ channel pore module. J Gen Physiol (in press)

Albertsen A, Hansen UP (1994) Estimation of kinetic rate constants from multi-channel recordings by a direct fit of the time series. Biophys J 67:1393–1403

Ashcroft FM (2006) From molecule to malady. Nature 440:440–447

Ball BF, Yeo GF, Milne RK, Edeson RO, Madsen BW, Sansom MSP (1993) Single ion channel models incorporating aggregation and time interval omission. Biophys J 64:357–367

Beckstein O, Biggin PC, Bond P, Bright JN, Domene C, Grottesi A, Holyoake J, Sansom MSP (2003) Ion channel gating: insights via molecular simulations. FEBS Lett 555:85–90

Bernèche S, Roux B (2005) A gate in the selectivity filter of K^+ channels. Structure 13:591–600

Blatt MR (2004) Membrane transport in plants. Blackwell Publishing Ltd, Oxford

Blunck R, Kirst U, Riessner T, Hansen UP (1998) How powerful is the dwell time analysis of multi-channel records? J Membr Biol 165:19–35

Börjesson SI, Elinder ÆF (2008) Structure, function, and modification of the voltage sensor in voltage-gated ion channels. Cell Biochem Biophys 52:149–174

Caceci MS, Cacheris WP (1984) Fitting curves to data: the simplex algorithm is the answer. BYTE 5(84):340–362

Colquhoun D, Hawkes AG, Srodzinski K (1996) Joint distributions of apparent open times and shut times of single ion channels and the maximum likelihood fitting of mechanisms. Phil Trans Roy Soc Lond A 354:2555–2590

Crouzy SC, Sigworth FJ (1990) Yet another approach to the dwell-time omission problem of single-channel analysis. Biophys J 58:731–743

Doyle DA, Cabral JM, Pfuetzner RA, Kuo A, Gulbis JM, Cohen SL, Chait BT, MacKinnon R (1998) The structure of the potassium channel: molecular basis of K^+ conduction and selectivity. Science 280:69–77

Draber S, Hansen UP (1994) Fast single-channel measurements resolve the blocking effect of Cs^+ on the K^+ channel. Biophys J 67:120–129

Draber S, Schultze R (1994) Correction for missed events based on a realistic model of a detector. Biophys J 66:191–202

Farokhi A, Keunecke M, Hansen UP (2000) The anomalous mole fraction effect in *Chara*: gating at the edge of temporal resolution. Biophys J 79:3072–3082

Feller W (1968) An introduction to probability theory and its applications, vol 1. Wiley, London

Fierz B, Reiner A, Kiefhaber T (2009) Local conformational dynamics in alpha-helices measured by fast triplet transfer. PNAS 106:1057–1062

FitzHugh R (1983) Statistical properties of the asymmetric random telegraph signal with application to single-channel analysis. Math Biosci 64:75–89

Fredkin DR, Rice JA (2001) Fast evaluation of the likelihood of an HMM: ion channel currents with filtering and colored noise. IEEE Trans Sig Proc 49:625–633

Freddolino PL, Liu F, Gruebele M, Schulten K (2008) Ten-microsecond molecular dynamics simulation of a fast-folding WW domain. Biophys J 94:L75–L77

Gillespie DT (1977) Exact stochastic simulation of coupled chemical reactions. J Phys Chem 81:2340–2361

Hansen UP, Keunecke M, Blunck R (1997) Gating and permeation models of plant channels. J Exp Bot 48:365–382

Hansen UP, Cakan O, Abshagen M, Farokhi A (2003) Gating models of the anomalous mole fraction effect of single-channel current in *Chara*. J Membr Biol 192:45–63

Hedrich R, Marten I (2006) 30-year progress of membrane transport in plants. Planta 224:725–739

Heinemann SH, Sigworth FJ (1988) Open channel noise. IV. Estimation of rapid kinetics of formamide block in gramicidin A channels. Biophys J 54:757–764

Heinemann SH, Sigworth FJ (1991) Open channel noise. VI. Analysis of amplitude histograms to determine rapid kinetics parameters. Biophys J 60:577–587

Huth T, Schroeder I, Hansen UP (2006) The power of two-dimensional dwell-time analysis for model discrimination,

temporal resolution, multichannel analysis and level detection. J Membr Biol 214:19–32

Huth T, Schmidtmayer J, Alzheimer C, Hansen UP (2008) 4-mode gating model of the inactivation of sodium channel Nav1.2a. Pflügers Arch 457:103–119

Jeon J, Voth GA (2008) Gating of the mechanosensitive channel protein MscL: the interplay of membrane and protein. Biophys J 94:3497–3511

Kienker P (1989) Equivalence of aggregated Markov models of ion-channel gating. Proc Roy Soc Lond Biol 236:269–309

Klieber HG, Gradmann D (1993) Enzyme kinetics of the prime K^+ channel in the tonoplast of *Chara*: selectivity and inhibition. J Membr Biol 132:253–265

Lehmann-Horn F, Jurkat-Rott K (1999) Voltage-gated ion channels and hereditary disease. Physiol Rev 79:1317–1372

Lu R, Alioua A, Kumar Y, Eghbali M, Stefani E, Toro L (2006) MaxiK channel partners: physiological impact. J Physiol 570: 65–72

Magleby KL, Song L (1992) Dependency plots suggest the kinetic structure of ion channels. Proc Roy Soc Lond B 249:133–142

Marsaglia G (2003) Random number generators. J Mod Appl Stat Methods 2:2–13

Michalek S, Wagner M, Timmer J (2000) A new approximate likelihood estimator for ARMA-filtered hidden Markov-models. IEEE Trans Sig Proc 48:1537–1547

Milne RK, Yeo GF, Madsen BW, Edeson RO (1989) Estimation of single channel kinetic parameters from data subject to limited time resolution. Biophys J 55:673–676

Miloshevsky GV, Jordan PC (2008) Conformational changes in the selectivity filter of the open-state KcsA channel: an energy minimization study. Biophys J 95:3239–3251

Moss BL, Magleby KL (2001) Gating and conductance properties of BK channels are modulated by the S9–S10 tail domain of the α subunit. A study of mSlo1 and mSlo3 wild-type and chimeric channels. J Gen Physiol 118:711–734

Qin F, Auerbach A, Sachs F (2000) Hidden Markov modelling for single-channel kinetics with filtering and correlated noise. Biophys J 79:1928–1944

Riessner T (1998) Level detection and extended beta distributions for the analysis of fast rate constants of markov processes in sampled data. Ph.D. thesis, Kiel, Germany and Shaker-Verlag, Aachen

Rothberg BS, Magleby KL (1999) Gating kinetics of single large-conductance Ca^{2+}-activated K^+ channels in high Ca^{2+} suggests a two-tiered allosteric gating mechanism. J Gen Physiol 114:93–124

Schroeder I, Hansen UP (2006) Strengths and limits of Beta distributions as a means of reconstructing the true single-channel current in patch clamp time series with fast gating. J Membr Biol 210:199–212

Schroeder I, Hansen UP (2007) Saturation and μs-gating of current indicate depletion-induced instability of the MaxiK selectivity filter. J Gen Physiol 130:83–97

Schroeder I, Hansen UP (2008) Tl^+-induced μs-gating of current indicate instability of the MaxiK selectivity filter as caused by ion/protein interaction. J Gen Physiol 131:365–378

Schroeder I, Hansen UP (2009) Interference of shot noise of open-channel current with the analysis of fast gating: patchers do not (yet) have to care. J Membr Biol. doi:10.1007/s00232-009-9183-3

Schroeder I, Huth T, Suitchmezian V, Jarosik J, Schnell S, Hansen UP (2004) Distributions-per-level: a means of testing level detectors and models of patch clamp data. J Membr Biol 197:49–58

Shafrir Y, Durell SR, Guy HR (2008) Models of voltage-dependent conformational changes in NaChBac channels. Biophys J 95:3663–3676

Sigworth FJ (1985) Open channel noise. I. Noise in acetylcholine receptor currents suggests conformational fluctuations. Biophys J 47:709–720

Tayefeh S, Kloss T, Thiel G, Hertel B, Moroni A, Kast SM (2007) Molecular dynamics simulation of the cytosolic mouth in Kcv-type potassium channels. Biochemistry 46:4826–4839

Tsushima RG, Kelly JE, Wasserstrom JA (1996) Characteristics of cocaine block of purified sacroplasmic recticulum calcium release channels. Biophys J 70:1263–1274

Venkataramanan L, Sigworth FJ (2002) Applying hidden Markov models to the analysis of single ion channel activity. Biophys J 82:1930–1942

Weise R, Gradmann D (2000) Effects of Na^+ on the predominant K^+ channel in the tonoplast of *Chara*: Decrease of conductance by blocks in 100 nanoseconds range and introduction of oligo- or poly-subconductance gating modes. J Membr Biol 175:87–93

White PJ, Ridout MS (1998) The estimation of rapid rate constants from current-amplitude frequency distributions of single-channel recordings. J Membr Biol 161:115–129

Yellen G (1984) Ionic permeation and blockade in Ca^{2+} activated K^+ channels of bovine chromaffin cells. J Gen Physiol 84:157–186

Yellen G (2001) Keeping K^+ completely comfortable. Nat Struct Biol 8:1011–1013

Zheng J, Sigworth FJ (1997) Selectivity changes during activation of mutant *Shaker* potassium channels. J Gen Physiol 110:101–117

Zheng J, Venkataramanan L, Sigworth FJ (2001) Hidden Markov model analysis of intermediate gating steps associated with the pore gate of *Shaker* potassium channels. J Gen Physiol 118:547–562

Zhou Y, Morais-Cabral JH, Kaufman A, MacKinnon R (2001) Chemistry of ion coordination and hydration revealed by a K^+ channel-Fab complex at 2.0 AA resolution. Nature 414:42–48

Zimmerman AL (2004) Capturing ion channel gating: a little salt on the tail does the trick. J Gen Physiol: 124:627–629